Secondary Structure Formation of a Transmembrane Segment in Kv Channels†

Jianli Lu and Carol Deutsch*

Department of Physiology, University of Pennsylvania, Philadelphia, Pennsylvania 19104-6085

Received February 28, 2005; Revised Manuscript Received April 14, 2005

ABSTRACT: Transmembrane segments in the intact voltage-gated potassium (Kv) channel are helical. To ascertain whether this helicity could first be manifested inside the ribosomal tunnel, we generated biogenic peptide intermediates of Kv1.3 and mass-tagged the cysteine-scanned S6 transmembrane segment using pegylation (PEG-MAL) and calmodulation (CaM-MAL). For reference, we created an extended peptide that was used as a "molecular tape measure" of the ribosomal tunnel and determined that the functional length of the tunnel is 99−112 Å. We demonstrate that the S6 segment forms a compact structure inside the ribosomal tunnel and that the N-terminal half of S6 compacts more than the C-terminal half of S6. These results bear on the earliest folding events during biogenesis of ion channels.

The essence of an ion channel is its conducting pore. Other regions of the channel protein modulate and gate the conducting pore, but it is the pore that is conserved throughout evolution. This critical domain is comprised of transmembrane segments, one from each of four subunits in the case of a voltage-gated potassium (Kv) channel. Yet, we know little about the mechanisms underlying acquisition of secondary, tertiary, and quaternary structure of these segments. In the intact mature Kv channel, these transmembrane segments are helical, whether assayed by tryptophan scanning (*1*−*4*), by alanine scanning (*5*), or, more recently, by direct crystallographic techniques (*6*). When could this helicity first be manifested? Could it be coincident with peptide synthesis of the transmembrane segment inside the ribosome? A peptide is synthesized at the peptidyl transferase center (PTC) in the cleft between the small and large ribosome subunits, and then, while still tethered at one end to the PTC, this "nascent" peptide wends its way along an exit tunnel as the nascent peptide is elongated. According to recent structure determinations, the tunnel is ∼100 Å long with a diameter of 10 Å near the entrance and 20 Å at the widest point near the exit site (*7*−*10*). These dimensions are compatible with secondary structure formation of Kv channel segments inside the ribosomal tunnel, as an α-helix is ∼10 Å in diameter (*11*). Secondary structure formation can be extremely fast (*12*) in comparison to peptide chain synthesis, which occurs at rates of 50−300 amino acids/min in cell-free systems and considerably faster in vivo (*13*). Thus, synthesis of a Kv channel monomer should take ∼1−2 min and is likely to be accompanied by secondary structure formation and compaction.

Indeed, there is evidence for compact structure formation inside the ribosome (e.g., refs *14*−*19*). The mechanisms promoting helix formation inside the ribosome are unknown, and could be similar to those in free solution. One suggestion proposes that nonpolar surfaces in the tunnel interact with hydrophobic sequences in the nascent peptide to promote helix formation (*20*) and that this interaction is sensitive to the length of the hydrophobic peptide, thus discriminating between transmembrane and secretory peptides (*15*). In addition, nascent peptides interact with ribosomal proteins and/or 23S rRNA, supporting the speculation that the ribosome itself actively promotes folding (*18*).

Tertiary and quaternary structures are also acquired early in biogenesis. Large polypeptides generally fold as small independent folding units (domains) and do so vectorially (*21*, *22*). Several proteins, particularly enzymes that can be monitored for functional activity as they emerge from the ribosome, fold into their tertiary structures while still bound to the ribosome (*16*−*18*, *23*, *24*). Quaternary structure acquisition is most commonly described for nascent soluble proteins (*25*), but has recently been reported for membrane proteins, specifically for the T1 domain of nascent Kv1.3 (*26*). Tertiary and quaternary structure formation occurs either concomitant with, or immediately after, secondary structure acquisition. If the latter occurs, then secondary structure could first be acquired inside the ribosomal tunnel.

To pursue this issue for specific Kv segments inside the ribosomal exit tunnel, we took the following approach. First, to calibrate the distance in the ribosomal tunnel through which the Kv1.3 segments move, we used a peptide known to be all-extended to create a molecular tape measure and determined the functional length of the tunnel. To poise the tape measure inside the ribosome, we generated biogenic intermediates that remain attached to the ribosome (*26*). The assay for these studies entailed a combination of pegylation, i.e., mass tagging a peptide with a large, polyethylene glycol maleimide (PEG-MAL, 5 kDa), and cysteine accessibility methods (*27*, *28*). A cysteine was engineered at various positions along the tape measure. A cysteine buried inside the tunnel is relatively inaccessible compared to a cysteine that has emerged from the tunnel, which can be mass-tagged with PEG-MAL and detected by a gel shift assay (*27*). If a fully extended peptide occupies 3.0−3.4 Å/amino acid,

† Supported by National Institutes of Health Grant GM 52302.

* To whom correspondence should be addressed: Department of Physiology, University of Pennsylvania, Philadelphia, PA 19104-6085. Phone: (215) 898-8014. Fax: (215) 573-5851. E-mail: cjd@mail.med.upenn.edu.

10.1021/bi050372q CCC: $30.25
Published on Web 05/14/2005

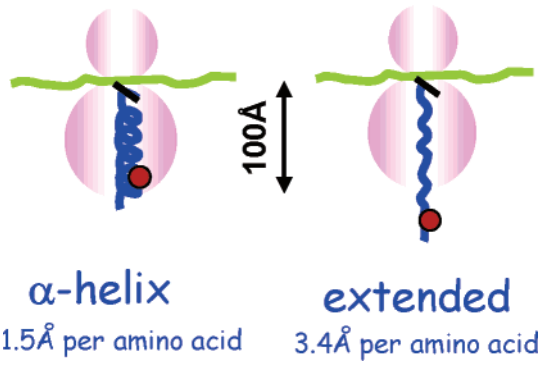

FIGURE 1: Engineered cysteine in two different secondary structures of a nascent peptide. The large and small subunits of the ribosome (pink) are depicted containing a nascent peptide (blue) and mRNA (green). In one case (left), the peptide is in a helical conformation; the other case (right) shows a nascent peptide in an extended conformation. The tRNA that is attached to the nascent peptide at the peptidyltransferase center (PTC) is represented as a thick black bar. An engineered cysteine is colored red. The anatomical length of the ribosomal exit tunnel is ~100 Å (*7*−*10*).

whereas an α-helix occupies 1.5 Å/amino acid (*11*), then an extended conformation would require only 33 amino acids to traverse 100 Å, whereas an α-helix would require ~67 amino acids (Figure 1). The length of the protein when it first emerges from the ribosome at the exit site should therefore reflect the secondary structure of the nascent peptide. In addition to PEG-MAL, we introduce a new mass-tagging reagent, bulky calmodulin maleimide (CaM-MAL), because it is a more stringent reagent for identifying inaccessible residues at a protein−protein interface or inside the ribosomal tunnel. To investigate Kv secondary structure formation inside the ribosomal tunnel, we chose the hydrophobic S6 transmembrane segment of Kv1.3. S6 is profoundly important in Kv channels because it lines the permeation pore and forms the activation gate (*29*). S6 is helical in mature Kv channels, but may contain a kink or hinge (*3*, *6*, *30*). Improper formation of this segment precludes channel expression and function, leading to channelopathies. To probe nascent S6 secondary structure, we measured the accessibility, using pegylation and calmodulation, of engineered cysteines in S6 residing in the ribosomal tunnel as a biogenic intermediate.

These new approaches extend the repertoire of tools and strategies with which to address mechanisms of protein folding and assembly and provide novel insights into channel biogenesis. We now report that the functional length of the ribosomal tunnel is ~99−112 Å and the N-terminal segment of S6 acquires a compact structure inside the ribosomal tunnel.

MATERIALS AND METHODS

Constructs and in Vitro Translation. Standard methods of bacterial transformation, plasmid DNA preparation, and restriction enzyme analysis were used. The nucleotide sequences of all mutants were confirmed by automated cycle sequencing performed by the DNA Sequencing Facility at the School of Medicine on an ABI 377 sequencer using Big dye terminator chemistry (ABI). The tape measure DNAs were sequenced throughout the entire coding region. All mutant S6 Kv1.3 DNAs were sequenced from S5 to the end of the C-terminus of the coding region. Engineered cysteines were introduced into pSP/Kv1.3/cysteine-free (*26*) using the QuikChange site-directed mutagenesis kit.

All constructs (tape measures and S6-containing peptides) begin at the N-terminus of Kv1.3 and end at the designated restriction site. All tape measure constructs, derived from the T1 domain of Kv1.3, including R62C(E64Q), F63C-(R62Q/E64Q), E64C, T65C, Q66C, Q72C, F73C(E75Q), and P74C(E75Q) mutations, were made in a Kv1.3 cysteine-free background. C71 is a native cysteine and was replaced with serine in the cysteine-free background. The second mutations, listed in parentheses, were carried out to remove charged side chains that might confound the kinetics of pegylation. The measured rates, therefore, reflect primarily accessibility. Two α-helices, α1 (from L67 to L70) and α2 (from P81 to R83) in the wild-type T1 domain, were deleted, and a new *Bst*EII digestion site was engineered at R101 using the QuikChange site-directed mutagenesis kit. Thus, all tape measure constructs have a molecular mass of ~11 kDa and appear at ~15 kDa on a NuPAGE Bis-Tris gel/MES running buffer.

An alanine replacement construct, Ala10, was made using the E64C tape measure as a template. Residues L91−N100 were replaced with 10 consecutive alanines to create a construct with two amino acids between the PTC and the C-terminus of the alanine sequence.

S6 transmembrane constructs contained engineered cysteines as a result of S429C, V428C, T419C, L418C, L411C, S410C, G409C, and V408C mutations and were made in an otherwise cysteine-free Kv1.3 background using the QuikChange site-directed mutagenesis kit. Residue C412 is a native cysteine. The *Nsp*HI restriction site at position 448 was used as a digestion site to make biogenic intermediates for studying the accessibility of S6 cysteines. Thus, all S6-containing constructs contain the first 447 residues of Kv1.3 and have a molecular mass of ~49 kDa.

Capped cRNA was synthesized in vitro from linearized templates using Sp6 RNA polymerase (Promega, Madison, WI). Linearized templates for Kv1.3 biogenic intermediates were generated using the *Bst*EII or *Nsp*HI enzyme. Proteins were translated in vitro with [^{35}S]methionine (2 μL/25 μL of translation mixture; ~10 μCi/μL of Express, Dupont/NEN Research Products, Boston, MA) for 1 h at 22 °C according to the Promega Protocol and Application Guide.

Gel Electrophoresis and Fluorography. All final samples were treated with 0.5−1 μl of 500 μg/mL RNase for 15 min at room temperature to digest tRNA and remove contaminating peptidyl-tRNA bands that would normally be present in all gels displaying samples derived from biogenic intermediates (*26*). Samples were mixed with NuPAGE sample buffer (1 M glycerol, 0.5 mM EDTA, 73 mM LDS, 141 mM Tris base, and 106 mM Tris-HCl) and heated at 70 °C for 10 min before being loaded onto the gel. Electrophoresis was performed using the NuPAGE system and precast Bis-Tris 10% or 4−12% gels and MES (50 mM) or MOPS (50 mM) running buffer (50 mM Tris base, 3.5 mM SDS, and 1 mM EDTA). Gels were soaked in Amplify (Amersham Corp., Arlington Heights, IL) to enhance ^{35}S fluorography, dried, and exposed to Kodak X-AR film at −70 °C. Typical exposure times were 16−30 h. Quantitation of gels was carried out directly using a Molecular Dynamics (Sunnyvale, CA) PhosphorImager, which is very sensitive and detects counts per minute that are not necessarily visualized in

autoradiograms exposed for 16−30 h. Gels treated with gelcode blue stain (Figure 2A) were first washed three times (5 min each time) with deionized water, stained for 1 h, washed three times with deionized water (20 min each time), and dried.

CaM-MAL Synthesis and Purification. Plasmid DNA (10−50 ng) containing P66C-calmodulin (P66C-CaM; a gift from Y. Goldman) was used to transform the competent cells from Stratagene [BL 21-Codon plus (DE3) RIL]. The next day, when the OD of the culture reached 0.8, 1 mM (final) IPTG was added to the bacteria to induce the gene. Cells were spun down and lysed with 50 mM Tris, 2 mM EDTA, 5 mM DTT, 100 mM NaCl, 1 mM PMSF, and 1× protease inhibitor cocktail (pH 7.5). The supernatant was loaded onto EDTA−phenyl-Sepharose columns and purified. Purified P66C-CaM was used to react with *o*-phenyldimaleimide (PDM, Sigma Chemical Co.) to make calmodulin maleimide (CaM-MAL). Specifically, a solution of P66C-CaM (50 μL, 1 mM) was slowly added dropwise (5 μL) to 500 μL of stirred buffer containing 20 mM Hepes, 100 mM NaCl, and 0.5 mM PDM for 1 h at 4 °C. A microcon filter system with a molecular mass cutoff of 10 kDa was used to remove free PDM and concentrate the CaM protein.

A priori, we might expect three different species of CaM: unmodified CaM, CaM-MAL, or a PDM-linked dimer (CaM-MAL-phenyl-MAL-CaM). However, we used reaction conditions (see above) that favored formation of CaM-MAL. To analyze the CaM species present, we used gelcode blue stain (Pierce) of a NuPAGE gel loaded with the reaction products pretreated with either of two different pegylating reagents. PEG-MAL reacts with cysteines and thus will detect CaM-P66C, whereas PEG-SH reacts with maleimides and thus will detect CaM-MAL. Each one of these reagents produces an ∼10 kDa gel shift when the protein is pegylated (*24*, *27*). The dimer would appear as a band at ∼34 kDa. As shown in Figure 2A, no such band is present in lane 3, indicating no CaM dimer was formed. Nor is unmodified CaM present (lane 4). CaM-MAL is the major species (>90%, lane 5).

To evaluate CaM-MAL's inaccessibility to small crevices at protein−protein interfaces and to ensure that CaM-MAL does not unwind or snake into a sterically hindered region, e.g., the ribosomal tunnel, where our nascent Kv1.3 peptide resides, we compared the kinetics and final extent of labeling for two categories of known cysteines, one that is freely accessible in Kv1.3 and one that is at a protein−protein interface. For the former, we used an exposed native cysteine in the T1 domain, C71; for the latter, we used R118C, a cysteine engineered at the T1−T1 intersubunit interface. R118C can be cross-linked to an apposing cysteine (D126C) in the T1−T1 interface. Both C71 and R118C have been characterized previously with respect to their pegylation kinetics and ability to be cross-linked (*26*, *27*). CaM-MAL readily modifies C71, at approximately the same rate as PEG-MAL when applied at the same concentrations (Figure 2B), but does not modify R118C as readily as PEG-MAL (Figure 2C). The ratio of rate constants (k_{PEG}/k_{CaM}) for modification of C71 is 1.23 ± 0.06 (n = 3). The rate constant for pegylation of R118C is 0.063 ± 0.004 M^{-1} s^{-1} (mean ± average error, n = 2); the rate of modification of R118C by CaM-MAL is too slow to measure (<6% labeled in 20 h at 1 mM CaM-MAL). These results confirm that the relative modification rates for PEG-MAL and CaM-MAL can be used to identify protein−protein interfaces. An accessible cysteine has a modification rate ratio (k_{PEG}/k_{CaM}) of ∼1, whereas a ratio of ≫1 suggests sterically hindered access of reagent to the cysteine. Examples of the latter could include a nascent peptide inside the ribosomal tunnel and/or hindrance at a protein−protein interface.

Pegylation and Calmodulation Measurements. As described previously (*27*), the translation product (5−10 μL) was centrifuged through a sucrose cushion [100 μL; 0.5 M sucrose, 100 mM KCl, 5 mM $MgCl_2$, 50 mM Hepes, and 1 mM DTT (pH 7.5)] for 20 min at 70 000 rpm at 4 °C to isolate ribosome-bound peptide. The pellet was resuspended on ice in 50 μL of buffer containing 100 mM NaCl, 5 mM Mg^{2+}, 20 mM Hepes, and 50 μM DTT (pH 7.2). Effective resuspension required careful (avoid bubble formation) and repetitive pipetting (>100 times). An equal volume of buffer containing 2 mM PEG-MAL (5 kDa, Nektar Therapeutics) was added (final PEG-MAL concentration of 1 mM) and incubated on ice for the appropriate times (five to six time points between 0 and 6 h) for time course experiments. Additional measurements of the final extent of labeling were carried out using two consecutive time points at 3 and 4 h or at 5 and 6 h. Reactions were terminated by addition of 100 mM DTT, followed by incubation of the mixture at room temperature for 10−15 min. Time course data were fit to a single- or double-exponential function to calculate the rate constants. For those experiments using constructs containing C408 and C429 that were carried out in the presence of membranes, initial centrifugation through a sucrose cushion was carried out for 5 min at 55 000 rpm. In these cases, membranes were solubilized with 0.05% dodecyl maltoside ($C_{12}M$). For those experiments using CaM-MAL (and the corresponding PEG-MAL control), the pellets were resuspended in 20 μL, and an equal volume of buffer containing 2 mM CaM-MAL or PEG-MAL was added.

RESULTS

A Molecular Tape Measure. To address whether transmembrane Kv segments acquire their secondary structure inside the ribosomal exit tunnel, we first had to determine the functional length of the ribosomal exit tunnel. For this purpose, we created a molecular tape measure, a peptide of known extended structure that remains attached to the ribosome (a nascent peptide), and then applied a variant of the substituted cysteine accessibility method (*27*, *28*). This method relies on modifying engineered cysteines with cysteine reagents. Here we used PEG-MAL, a reagent previously introduced by our laboratory to elucidate Kv1.3 topology (*27*) and tertiary folding (*24*). A portion of the Kv1.3 T1 sequence (residues 52−101) serves as an all-extended molecular tape measure (Figure 3A). The Kv1.3 T1 sequence, which is 95% identical with the Kv1.1a T1 sequence, for which there is a high-resolution crystal structure (*31*), was modified by deleting two small α-helices (α1 and α2, containing four and three residues, respectively) and inserting a *Bst*EII digestion site at the C-terminal position just after residue R101. This is the PTC attachment site of the tape measure. The engineered *Bst*EII digestion site produced a serine at position 102 and thus a 95-amino acid long nascent chain, the C-terminal portion of which is the tape measure residing within the ribosomal exit tunnel. The

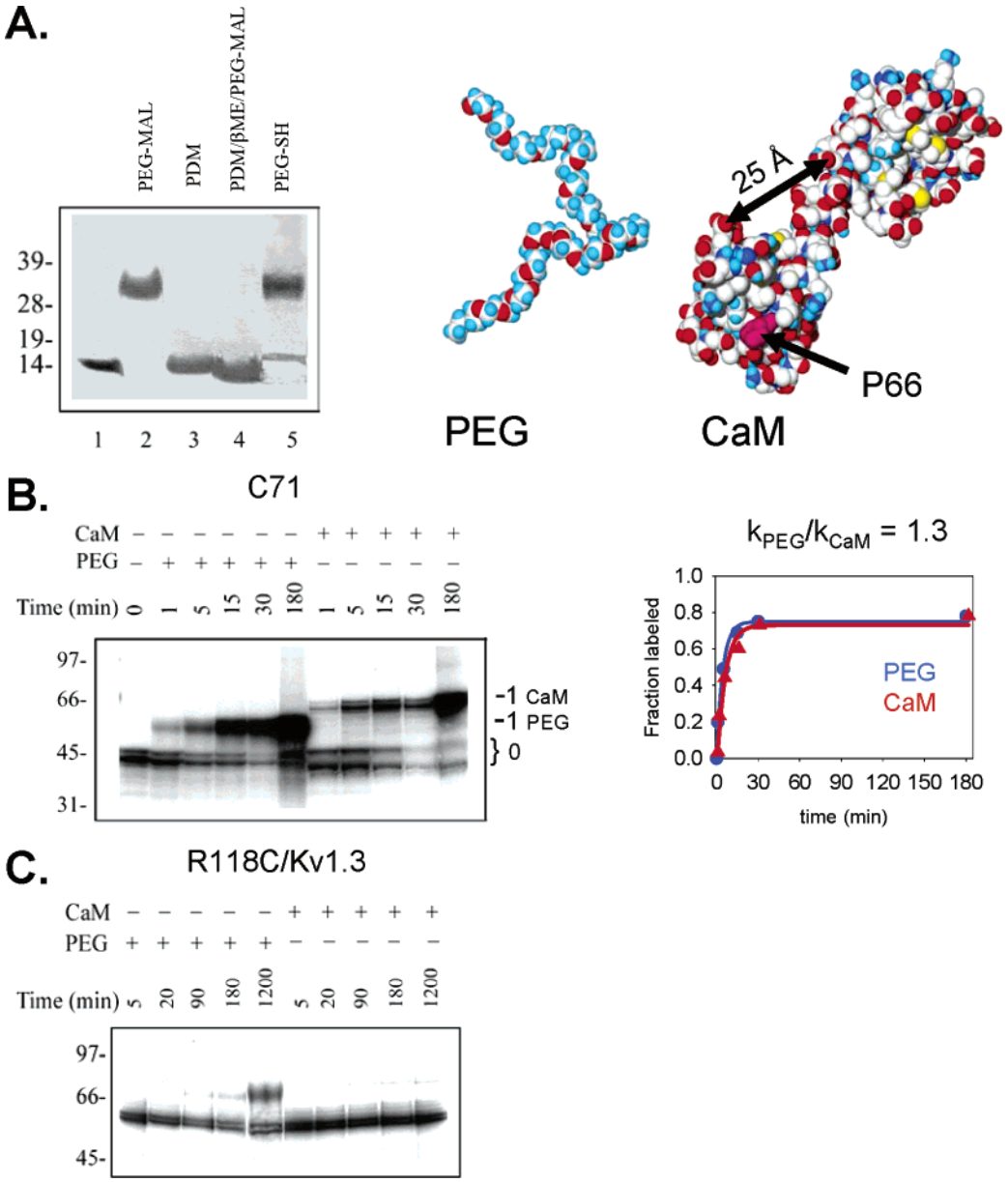

FIGURE 2: Comparison of PEG-MAL and CaM-MAL. (A) Synthesis of CaM-MAL and structures of PEG-MAL and CaM-MAL. Left: Using PEG-MAL (20 mM) and PEG-SH (20 mM) according to Kosolapov and Deutsch (*24*) and Lu and Deutsch (*27*), the gel illustrates that CaM was completely labeled with PDM to produce CaM-MAL. PEG-MAL was used to assess free cysteines in P66C-CaM, and PEG-SH was used to assess free maleimides in PDM-modified P66C-CaM. Lane 1 shows unmodified CaM at 17 kDa; lane 2 shows pegylated CaM. Lane 3 shows CaM modified with PDM (0.5 mM) to give the expected parent molecular mass species. Notice the complete absence of any dimeric species at 34 kDa, which theoretically could have occurred if two CaM molecules were cross-linked by a covalent link with PDM. Lane 4 shows that CaM, first modified with PDM, then fully reduced with β-mercaptoethanol, and treated with PEG-MAL to assess residual unmodified P66C, is completely labeled with PDM and remains at the parent molecular mass. Lane 5 shows that CaM, first modified with PDM and then treated with PEG-SH to assess free maleimides, has shifted, indicating that CaM-MAL is virtually the only species (>90%) present. Gels were 10% NuPAGE Bis-Tris with MES running buffer, stained with gelcode blue stain. Numbers to the left of the gels are molecular mass standards. Middle: The PEG structure, drawn with Chem3D, shows 32 of the 113 ethylene glycol repeats. Right: The structure of CaM is Protein Data Bank entry 1CLL viewed with DeepView. Proline 66 is colored magenta. Both molecules are displayed as standard CPK renderings on the same scale. (B) Kinetics of modification of an exposed cysteine. The time course of modification by PEG-MAL or CaM-MAL (1 mM) was measured for a freely accessible native cysteine (C71) in the cytosolic T1 domain of Kv1.3 translated in the presence of microsomal membranes. This construct, an intermediate attached via a native *BstE*II digestion site to tRNA at the PTC, is 43 kDa. It has been rendered cysteine-free except for the native C71, which is at a protein−aqueous interface (*27*, *31*). The left panel shows the unmodified and singly modified protein at the indicated times. A 4−12% Bis-Tris gel with MOPS running buffer was used in the NuPAGE system. The doublets are due to glycosylated protein in the presence of microsomal membranes and are together labeled as "0" to signify unpegylated protein. Singly pegylated protein is labeled as "1 PEG", and singly calmodulinated protein is labeled "1 CaM". The right panel shows the calculated fraction labeled with PEG-MAL or CaM-MAL vs time. Data were fit to a single exponential. The calculated rate constants were 3.7 and 2.8 M^{-1} s^{-1} for modification by PEG-MAL and CaM-MAL, respectively. The ratio of rate constants is 1.3. (C) Kinetics of modification of a buried cysteine. The time course of modification was measured for the relatively inaccessible R118C, a cysteine engineered at the T1−T1 intersubunit interface. This construct is a full-length Kv1.3 (58 kDa) released into the bilayer of the microsomal membrane with the T1 domain in the cytosol. R118C has been characterized previously with respect to its pegylation kinetics and ability to be cross-linked to another T1 cysteine in an adjacent subunit (*26*, *27*). Pegylation is slow (0.06 M^{-1} s^{-1}), whereas modification by CaM-MAL is immeasurably slow and cannot yield a rate constant.

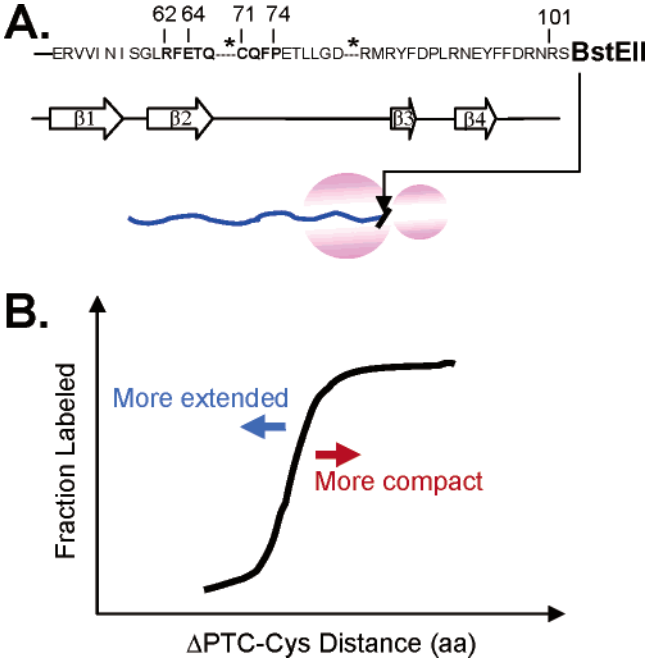

FIGURE 3: Molecular tape measure. (A) Tape measure created from the Kv1.3 T1 domain. The sequence of the tape measure is shown, including positions of cysteine substitutions (bold). A *Bst*EII restriction site, engineered at position 101, introduces a serine at position 102 and is the site of attachment to tRNA at the PTC. This construct produces a 95-amino acid nascent peptide (appears at ~15 kDa on the gel), the C-terminal portion of which is the tape measure residing within the ribosomal exit tunnel. Residue C71 is a native cysteine in Kv1.3. Dashes represent deleted residues that form α-helices in the native sequence (α1 and α2, containing four and three residues, respectively). Segments known to be *β*-strands or extended according to the crystal structure are indicated under the sequence. (B) Cartoon of the final extent of labeling of the tape measure vs the distance from the PTC (in number of amino acids, aa). If a nascent peptide is more extended than the tape measure, fewer amino acids will be necessary to traverse the tunnel and labeling will be more complete with fewer amino acids between the cysteine and the PTC. If a nascent peptide is compact, more amino acids will be necessary to detect equivalent labeling.

N-terminal end is outside the ribosome. Although final levels of modification should be independent of the electrostatics, the rates could be influenced by nearby charged residues, which will affect the extent of ionization of the thiol in forming the reactive thiolate ion in the pegylation reaction. To obviate this complication, we mutated nearby arginines and glutamates (residues 62, 64, and 75) to neutral glutamine when necessary (see Materials and Methods). This sequence of T1 has a predicted nonhelical structure [<3% helix propensity according to the AGADIR algorithm (*32*)] and according to the crystal structure of Kv1.1a is all-extended. Single cysteines were engineered separately into the tape measure at positions 62−66 and 72−74, according to the numbering in the wild-type Kv1.3 T1 domain, and are shown in Figure 3A. Residue 71 is a native cysteine and was also used as a modifiable cysteine in the tape measure background. When a cysteine was introduced elsewhere, C71 was mutated to serine. Each tape measure containing a single cysteine was created as a biogenic intermediate that remains attached to the ribosome because the mRNA made from truncated *Bst*EII-cut cDNA lacks a stop codon (*26*). Each intermediate was translated in a cell-free, membrane-free rabbit reticulocyte system with added [^{35}S]methionine and then pegylated according to previous protocols (*27*) with some modifications to permit accurate determination of rate constants and the final extent of pegylation. The dependence of the fraction pegylated on the number of amino acids between the PTC and the engineered cysteine for any given nascent peptide can be compared to that for the tape measure (Figure 3B) and will indicate whether the peptide is more compact (right shift of the curve) or less compact (left shift of the curve) than the tape measure.

For three examples, C64, C65, and C73, Figure 4 shows the time course of pegylation and fit of the data to the single-exponential function expected for the reaction. The lower band in the gels (labeled "0") represents the unmodified nascent peptide and the upper band (labeled "1") the singly pegylated nascent peptide. Both C64 and C65, which are 32 and 31 amino acids from the PTC, respectively, are pegylated to a maximum of ~77 and 51%, respectively. However, cysteine 73, which is 27 amino acids from the PTC, is barely pegylated after 3 h in 1 mM PEG-MAL (<5%), and the modification rate is too slow to permit an accurate determination of the rate constant. Both rates and the final extent of labeling vary among the different substituted cysteines and increase monotonically with the distance of the cysteine from the PTC (Figure 5A), suggesting that the relative inaccessibility is due to residence inside the ribosome tunnel. The lack of pegylation of cysteines 71−74 could be due to their inaccessibility and/or low reactivity. However, our experiments show that these cysteines are still reactive because NEM pretreatment blocks subsequent pegylation of the SDS detergent-solubilized nascent peptide (data not shown). Therefore, relative pegylation primarily reflects accessibility.

Because peptides with cysteines at position 62 or 63 have an 80% final extent of labeling with rates of 0.7 M^{-1} s^{-1}, the threshold length for exit from the tunnel is ~33 amino acids from the PTC. This corresponds to a tunnel length of 99−112 Å, assuming 3.0−3.4 Å per amino acid for an all-extended peptide. A minimum of only five to six amino acids is required to traverse the distance between an inaccessible region and a fully accessible region, corresponding to a distance of ~15−20 Å for an all-extended peptide. The distribution of labeled and unlabeled cysteines likely reflects a mixed population of nascent peptides in which one fraction has accessible cysteine side chains and the other does not (see the discussion below about calmodulation). The relative fraction of the cysteine-accessible population decreases as the reactive residues are situated deeper within the ribosomal tunnel. On the basis of both the extent and rates of labeling, we locate the positions of the cysteines along the exit tunnel as shown in Figure 5B.

To confirm that the tape measure/accessibility method can be used to faithfully determine compact structure inside the ribosome, we inserted a molecular "spring" into the tape measure; i.e., 10 alanines (Ala10) were substituted for 10 tape measure residues (Figure 6, bottom). Alanine has a high helix propensity: 10 successive alanines gives a predicted fractional helicity of 0.30 [AGADIR algorithm (*32*)], and polyalanine traverses the ribosomal tunnel as an α-helix (*33*, *34*). Helix formation will produce a more compact nascent peptide when an Ala sequence replaces an all-extended segment of the tape measure that lies between C64 and the PTC. Compaction of the nascent peptide will retract border residue C64 inside the ribosomal exit tunnel so that the cysteine is no longer as accessible (Figure 6). This scenario

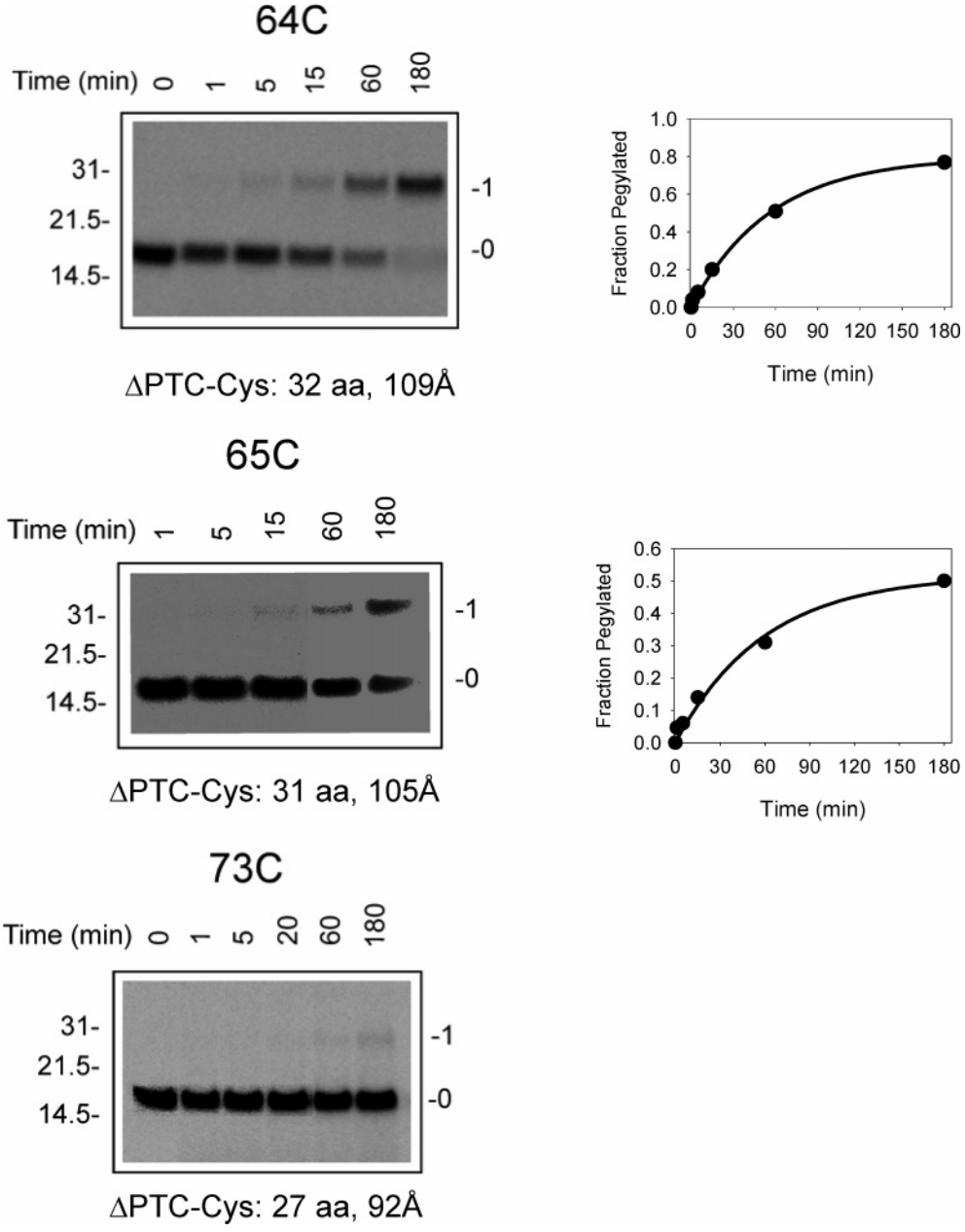

FIGURE 4: Kinetics of modification of tape measure cysteines. Left gels: Time course of pegylation. Tape measures (described in the legend of Figure 3) containing cysteines located 32 (C64), 31 (C65), and 27 (C73) residues from the PTC (ΔPTC-Cys) were translated and labeled with [^{35}S]methionine in a rabbit reticulocyte system. Translation products were incubated with PEG-MAL (1 mM), quenched, and assayed on a gel, as described previously (*27*). Below each gel is shown the ΔPTC [calculated as the number of amino acids from the PTC (starting with engineered S102) to, and including, the indicated cysteine] and the distance (angstroms) if all ΔPTC-Cys residues are in an all-extended conformation, assuming 3.4 Å per residue. Gels were 10% NuPAGE Bis-Tris with MES running buffer. Numbers to the left of the gels are molecular mass standards; numbers to the right indicate unpegylated (0) and singly pegylated (1) protein. Right plots: Time course of fraction of individual cysteines pegylated. Pegylation data shown in the left panels were used to calculate counts per minute in band 1 divided by the sum of the counts per minute in bands 1 and 2, plotted at the indicated times, and fit to a single-exponential function. Rate constants for modification of C64 and C65 are 0.30 and 0.28 M^{-1} s^{-1}, respectively.

will be manifest as a decrease in the final extent of pegylation of C64. Figure 6 indicates that Ala10 gives a lower final extent of pegylation and an immeasurably slower rate. This result suggests that the combined use of the tape measure and accessibility measurements of nascent peptides faithfully reports compact structure formation of a nascent peptide inside the ribosomal exit tunnel.

A More Stringent Probe of Accessibility. Before applying our accessibility methods to the S6 transmembrane segment, we developed a more stringent accessibility assay using a bulkier mass tag, calmodulin maleimide (CaM-MAL), and used this reagent to verify our results with PEG-MAL. CaM is a 17 kDa globular protein, with molecular dimensions of ~25 Å × 68 Å, that lacks native cysteines (Figure 2A). We used a P66C mutant of CaM to make CaM-MAL, reasoning that because residue 66 is in the middle of the CaM protein primary sequence, it is unlikely to unwind and project its MAL moiety into the ribosomal exit tunnel. This is in contrast to the PEG-MAL, which is an unstructured linear polymer (113 ethylene glycol repeats) with a "thickness" of ~3 Å (Figure 2A) capable of snaking up into the ribosomal tunnel. CaM-MAL does not label cysteines at protein−

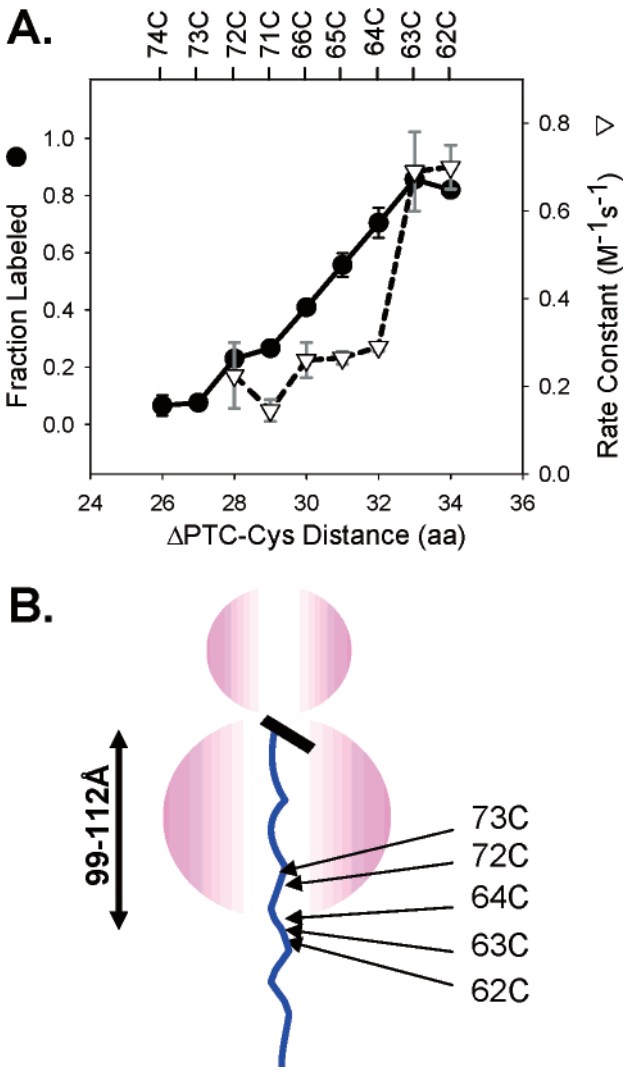

FIGURE 5: Accessibility of the tape measure. (A) Calculated final extent of modification and modification rate constants vs distance from PTC. PEG-MAL (1 mM) was used in replicate (three or four) experiments to obtain fraction labeled (●) at 3−6 h for all tape measure constructs depicted in Figure 3A. Data are means ± the standard deviation. Rate constants (▽) are derived from duplicate experiments and presented as means ± the average deviation. Results were plotted against the number of amino acids from the PTC to (and including) the labeled cysteine (ΔPTC-Cys). The additional numbers above the plot refer to the original Kv1.3 positions. (B) Assignment of cysteine locations. Each cysteine is shown to reside within or outside the ribosome, according to the results depicted in panel A. The calculated distance from C63 to the PTC is 99−112 Å, assuming a range of values of 3.0−3.4 Å per residue for an all-extended conformation of the peptide. The nascent peptide chain is not drawn to scale.

protein interfaces, whereas PEG-MAL can label such cysteines, albeit at slower rates than freely accessible cysteines (Figure 2B,C; see Materials and Methods).

We measured the modification of C65 in the tape measure with CaM-MAL. The rate was too slow to measure accurately, and the total extent of labeling, <5%, was unchanged over a period of time from 90 min to 5 h (data not shown). These results confirm that C65 resides within the tunnel, is only moderately accessible to PEG-MAL (final extent of pegylation of 50%), but is not accessible to the larger CaM-MAL, a 1 order of magnitude difference in pegylation versus calmodulation. These results eliminate the interpretation that 50% pegylation of C65 is due to 50% of the protein residing outside the tunnel and 50% inside. Rather, the 50% pegylation is due to some kind of heterogeneity inside the tunnel. Moreover, the lack of calmodulation of C65, as well as the inaccessibility of C429 (see below), indicates that the nascent peptide remains attached to the ribosome during the modification reaction. If peptide were released, it would be labeled by CaM-MAL. The results show the peptide is unlabeled until it is deliberately released from the ribosome with RNase (see below; Figure 8C,D).

Kv1.3 Transmembrane Segment, S6. With these tools in hand, we performed an accessibility assay of the S6 transmembrane segment of Kv1.3 using pegylation and calmodulation to determine whether S6 achieves a compact structure within the ribosome. Figure 7 shows the sequence of S6, the substituted cysteines in the S6 segment, as well as the restriction site at position 448 used to generate biogenic intermediates. This produces an ~49 kDa nascent peptide of Kv1.3 (residues 1−447), which poises S6 inside the ribosomal tunnel. Cysteines were engineered at positions in S6 between (and including) residue 408, at the N-terminal end of S6 on the extracellular (lumenal) side of the plasma (ER) membrane, and residue 429, at the C-terminal end of S6 on the cytoplasmic side of the membrane. Several issues were considered in our experiments. First, in the presence of ER membranes, residues that have emerged from the ribosomal tunnel will be either inside the translocon or

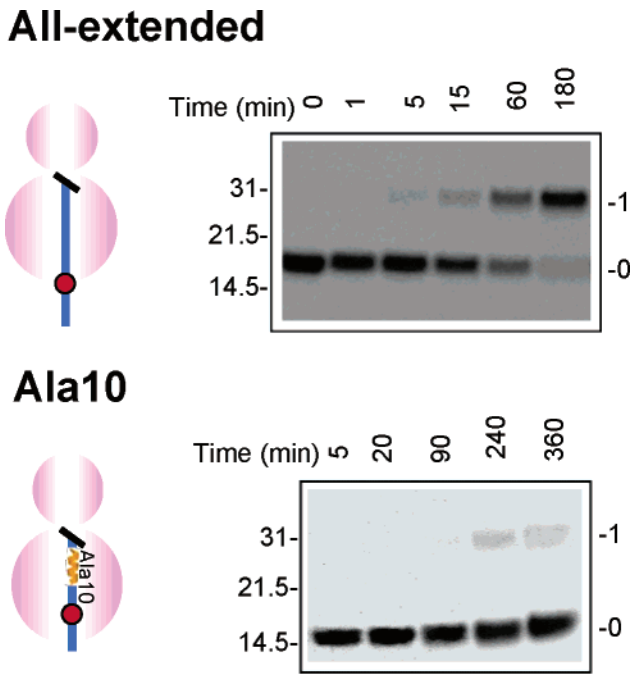

FIGURE 6: Tape measure and spring. The predicted locations of C64 in an all-extended tape measure (top left) vs that in Ala10 (bottom left), a C64-containing tape measure in which 10 residues have been replaced with 10 alanines, are shown as red circles. The polyalanine segment is presumed to be compact inside the ribosome. Replacement of tape measure residues with alanines causes C64 to be retracted into the ribosome. The nascent chain is colored blue and is not drawn to scale. The 10 substituted alanines are shown as an orange helix. The time course of pegylation of C64 was determined for the extended tape measure (top right) and the Ala10 tape measure (bottom right). Each construct was separately translated, pegylated, and fractionated on gels as described in the legend of Figure 4. Gels were 10% NuPAGE Bis-Tris with MES running buffer. Numbers to the left of the gels are molecular mass standards; numbers to the right indicate unpegylated (0) and singly pegylated (1) protein.

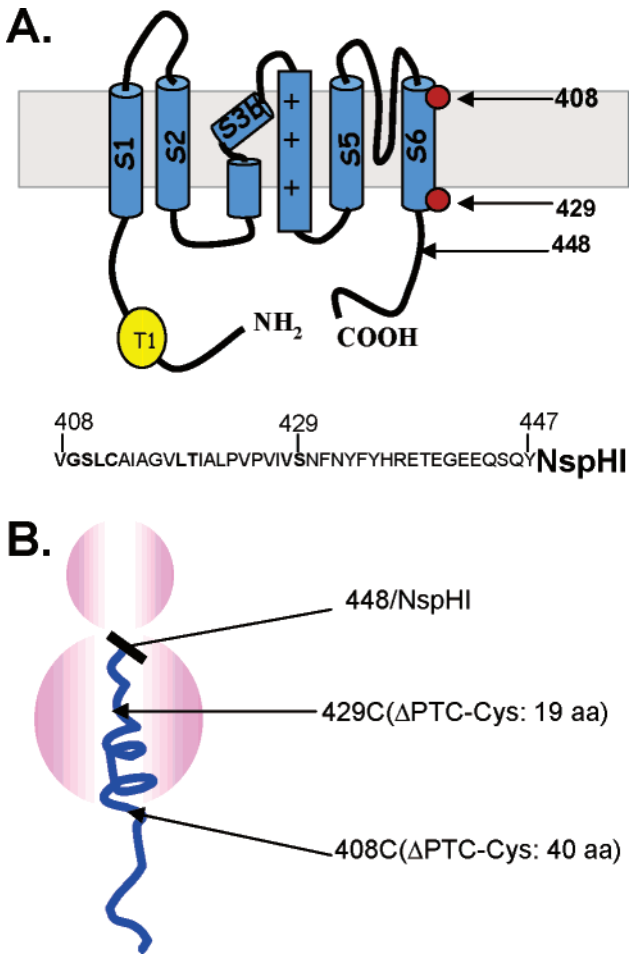

FIGURE 7: S6 Segment of Kv1.3. (A) Location of engineered cysteines in S6. Residues C408 and C429 are depicted at the N-terminal and C-terminal ends, respectively, of S6 (red circles). The chosen restriction site, *Nsp*HI, is at position 448 in the proximal C-terminus. Thus, this construct contains residues 1−447 of Kv1.3 and produces a 49 kDa nascent peptide. The sequence of S6 in Kv1.3 is indicated, as are the residues that were substituted one at a time with cysteine (bold) and pegylated in the translated Kv1.3 intermediate. (B) Predicted location of C429 and C408 in the *Nsp*HI-cut biogenic intermediate attached to the ribosome. The distance of the engineered cysteine from the PTC is shown in parentheses. Residue C429 is only 19 amino acids from the PTC and is predicted to be inside the ribosome. Residue 408 is 40 amino acids away, and its location depends on its secondary structure. The nascent peptide chain is not drawn to scale.

emergent and in the ER lumen. In both cases, the residue will be inaccessible to cysteine-modifying reagents in the intact system. Second, in the absence of ER membranes, all residues that have completely transited the ribosomal exit tunnel will be accessible for labeling, regardless of whether they ultimately reside in the cytoplasm or in the lumenal compartment, and provided that they are not hindered by accessory proteins. Third, nascent peptide released into the bilayer (with puromycin or RNase) will render cytoplasmic cysteines accessible for labeling, but not ER lumen-facing cysteines. In both cases, subsequent solubilization of the bilayer will make all the S6 cysteines accessible. Fourth, solubilization of the nascent peptide attached to the ribosome in a nondenaturing detergent, dodecyl maltoside ($C_{12}M$), leaves the ribosome−translocon−nascent peptide complex intact but dissolves the membrane. Thus, $C_{12}M$ leaves cysteines located inside the ribosome or translocon inaccessible while rendering those in the lumen or cytoplasm accessible. On the basis of these considerations, the appropriate conditions were used to probe the location of C429 and C408 in the ribosome−translocon−nascent peptide complex.

In the intact ribosome−translocon−nascent peptide complex (i.e., in the presence of microsomal membranes), residue C408 ultimately resides in the ER lumen before trafficking to the plasma membrane. Therefore, we translated the C408 nascent peptide in the presence of membranes and solubilized the sample in $C_{12}M$ prior to determining rates and final extent of labeling by PEG-MAL and CaM-MAL (Figure 8A). Residue C408 in the $C_{12}M$-solubilized membrane preparation is only labeled 20% due to the intact ribosome−translocon−peptide complex in $C_{12}M$. If the solubilized sample is released from the ribosome, 80% labeling occurs (Figure 8B), which is similar to the labeling achieved in the absence of membranes (see Figure 9A). We therefore locate C408, which is 40 amino acids from the PTC, in an extraribosomal compartment, i.e., the translocon.

In contrast to residue C408, residue C429 is inaccessible in the absence of detergent (Figure 8C, left gel), and even after solubilization in the nondenaturing detergent $C_{12}M$ (Figure 8C, right gel). The final extent of labeling by PEG-MAL and CaM-MAL is <5% in both cases, and modification rates are too slow to be measured. This lack of labeling is not due to a loss of reactivity of the cysteine in the ribosomal tunnel, as *N*-ethylmaleimide, a small, membrane-permeant reagent, and 4-acetamido-4-maleimidylstilbene-2,2-disulfonic acid, a small and charged, membrane-impermeable reagent, each can label C429 in the tunnel and block subsequent pegylation after release of the peptide with RNase (0.01 μg/μL for 20 min) and denaturation with SDS (1%, 20 min; data not shown). Moreover, both PEG-MAL and CaM-MAL were able to label C429 after the nascent peptide was solubilized in $C_{12}M$ and then released from the ribosome (Figure 8D), yielding final extents of labeling of 60 and 68%, respectively. We therefore locate C429, which is only 19 amino acids from the PTC, deep inside the ribosomal exit tunnel.

The results of a cysteine scan along S6, using PEG-MAL in the absence of membranes, are shown in Figure 9A. Residue C428 is as inaccessible to PEG-MAL as C429, and residues C409 and C408 are labeled equally well (80%) and therefore appear to be extraribosomal. There is a monotonic increase in the apparent accessibility between positions 419 and 409 (solid green line). The rates of pegylation also vary in a monotonic fashion (dashed green line), consistent with the increasing accessibility with the increasing distance of the cysteine from the PTC. A comparison between S6 and the tape measure of the relative length-dependent extent of pegylation will indicate whether S6 acquires secondary structure (see Figure 3B). Figure 9A shows that the length-dependent extent of pegylation for S6 (green curve) is shifted to the right of the tape measure (black curve; taken from Figure 5A) for the N-terminal half (residues 408−418) of S6, indicating that the N-terminal half of the S6 segment acquires a compact structure inside the ribosomal tunnel, whereas the C-terminal half of S6 and the proximal C-terminus (residues 419−448), which coincides with the tape measure, do not (Figure 9B; see the Discussion). The data for the tape measure and S6 cross at approximately a ΔPTC-cysteine distance of 29−30 residues. It takes five residues

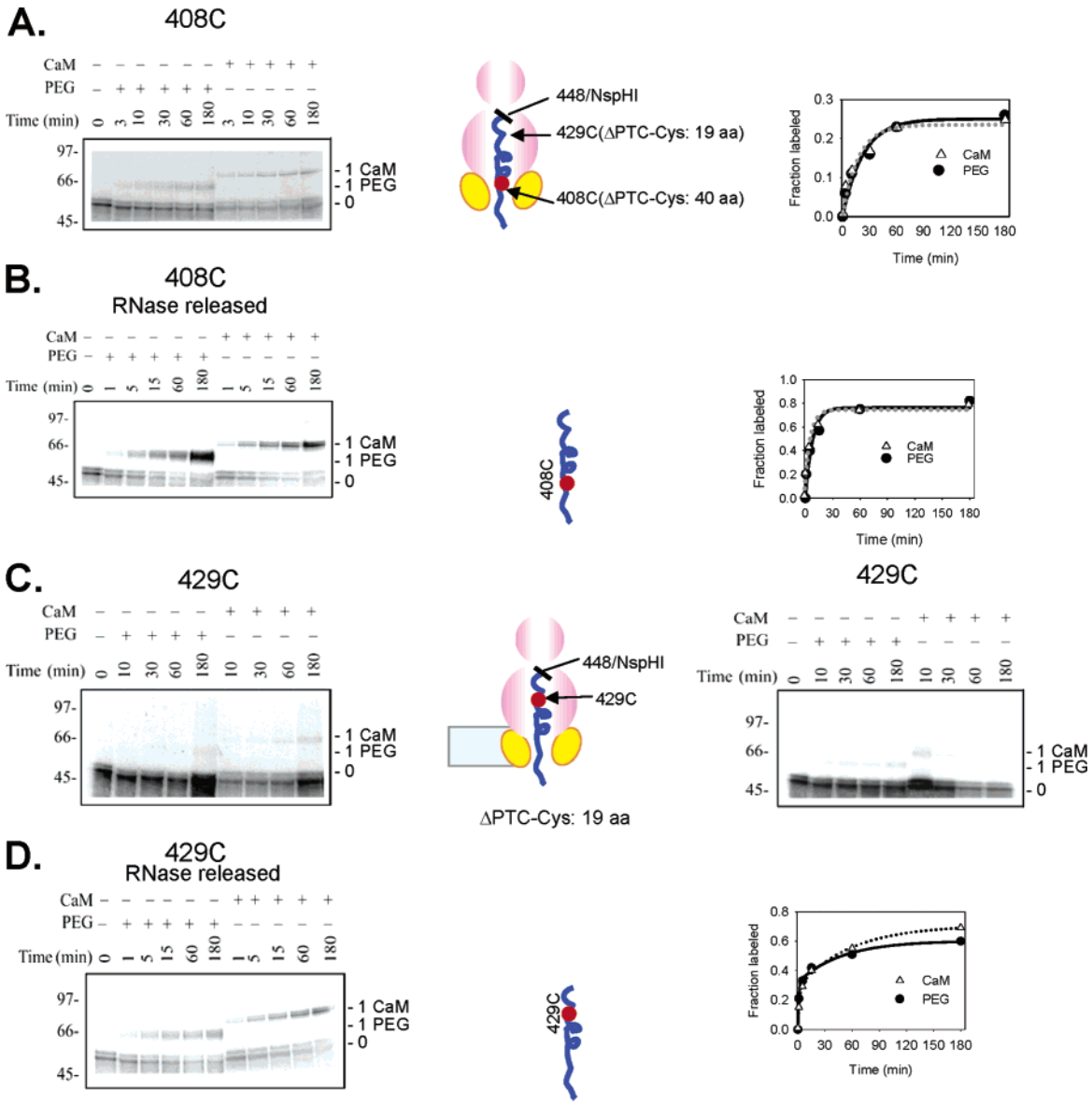

FIGURE 8: Accessibility of S6 residues C408 and C429. (A) Time course of PEG-MAL and CaM-MAL modification of the solubilized C408 peptide. A 448/*Nsp*HI-cut Kv1.3 construct containing only one cysteine, C408, was translated in the presence of microsomal membranes to give an ~49 kDa nascent peptide. The product was solubilized with nondenaturing detergent, $C_{12}M$, prior to modification of the nascent peptide, pegylated at the indicated times, and fractionated on a NuPAGE gel. The nascent peptide (blue) and cysteine 408 (red) are shown in the cartoon at the right. The yellow ovals represent the translocon to which the ribosome is directly attached. Right plot: The fraction modified was plotted for the indicated times and fit with a single-exponential function to give rate constants of 0.75 and 0.83 M^{-1} s^{-1} for modification by PEG-MAL and CaM-MAL, respectively. The ratio of rate constants is 0.9. The final fractions labeled by PEG-MAL and CaM-MAL were 0.26 and 0.25, respectively. (B) PEG-MAL and CaM-MAL modification of the released C408 peptide. The peptide generated in A was solubilized in $C_{12}M$ and released from the ribosome with RNase (5 μg/mL), modified, and fractionated on a NuPAGE gel. The released peptide (blue) and cysteine 408 (red) are shown in the cartoon. Right plot: The fraction modified was plotted for the indicated times and fit with a single-exponential function to give rate constants of 2.2 and 2.7 M^{-1} s^{-1} for modification by PEG-MAL and CaM-MAL, respectively. The ratio of rate constants is 0.81. The final fractions labeled by PEG-MAL and CaM-MAL were 0.82 and 0.77, respectively. (C) Time course of PEG-MAL and CaM-MAL modification of C429. Left gel: A 448/*Nsp*HI-cut Kv1.3 construct containing only one cysteine, C429, was translated in the presence of microsomal membranes to give an ~49 kDa nascent peptide. The product was modified with either PEG-MAL or CaM-MAL in the absence of detergent (left) or presence of $C_{12}M$ (right). The final extent of labeling by PEG-MAL and CaM-MAL is <5% in both cases, and the modification rates are too slow to measure. The cartoon depicts the experimental system in the absence and presence of detergent: the nascent peptide (blue) and cysteine 429 (red) are shown in the ribosome. The yellow ovals represent the translocon to which the ribosome is directly attached. The gray area represents the membrane, which is present in the experiments in the left panel, but solubilized, and therefore absent, in the right panel. Time course of PEG-MAL and CaM-MAL modification of the solubilized C429 peptide. Right gel: The product generated in C was solubilized with nondenaturing detergent, $C_{12}M$, prior to modification. Again, the final extent of labeling by PEG-MAL and CaM-MAL is <5% in both cases, and the modification rates are too slow to measure. (D) PEG-MAL and CaM-MAL modification of the released C429 peptide. Left gel: The peptide generated in C was solubilized in $C_{12}M$, released from the ribosome with RNase (5 μg/mL), and modified. The released peptide (blue) and cysteine 429 (red) are shown in the cartoon. Right plot: Modification data shown in the gel on the left were calculated as described in the legend of Figure 4 and fit to a double-exponential function. The calculated rate constants were 16.6 (0.32) and 0.35 (0.28) M^{-1} s^{-1} for modification by PEG-MAL and 10.1 (0.28) and 0.29 (0.42) M^{-1} s^{-1} for modification by CaM-MAL. The ratios of the fast and slow rate constants are 1.6 and 1.2, respectively. The final extents of pegylation are 0.60 and 0.68, respectively. Gels shown in panels A−D were 4−12% Bis-Tris with MOPS running buffer. In panels A−D, the nascent peptide chain is not drawn to scale.

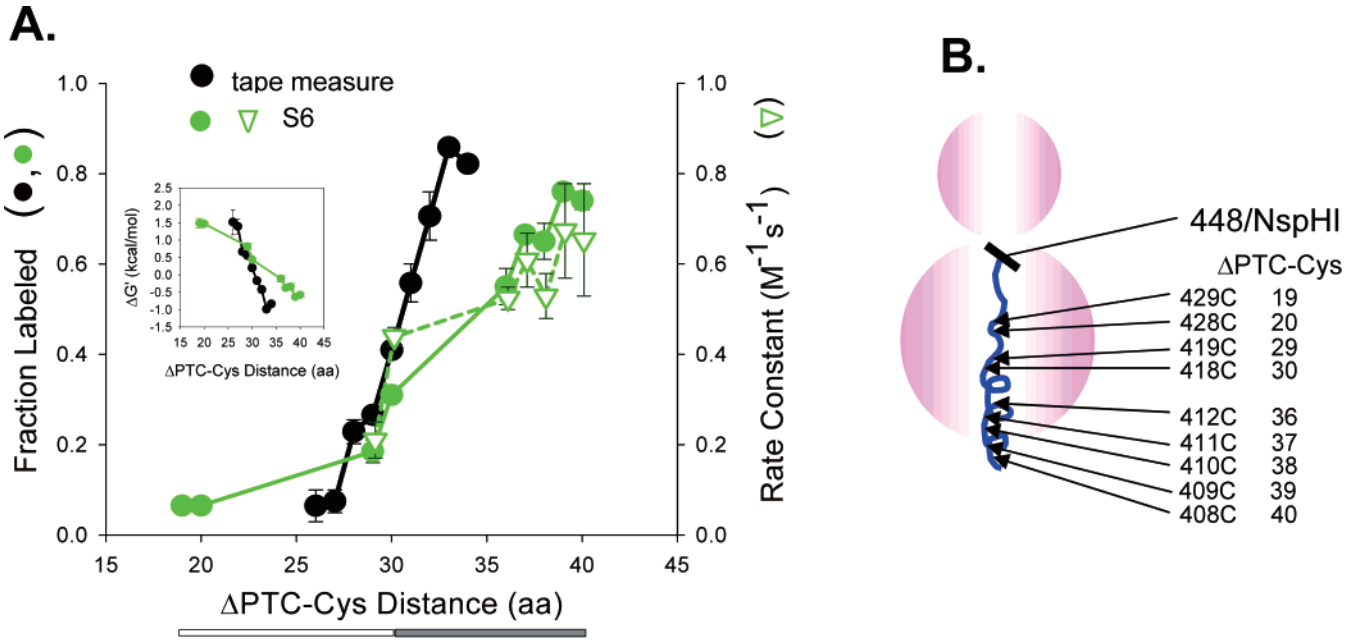

FIGURE 9: Accessibility of S6 residues. (A) Final extent of modification and modification rate constant vs the distance from PTC for S6 residues. Results of an accessibility scan of S6 using PEG-MAL are plotted against the number of amino acids from the PTC to (and including) the labeled cysteine. All S6 constructs contain residues 1−447 of Kv1.3 (~49 kDa) and were translated in the absence of membranes. The final extent of pegylation is shown as green circles (mean ± average deviation; $n = 2$); rate constants are shown as inverted triangles (mean ± average deviation; $n = 2$). The tape measure results from Figure 5A are also plotted (black circles). Predicted helical propensity was calculated for S6 residues 408−429 using the AGADIR algorithm and is shown on a relative scale below the *x*-axis (shaded area is helical). The inset shows the dependence of the apparent free energy on chain length. An apparent free energy, $\Delta G'$, was calculated as described in the text from pegylation data shown in panel A for the tape measure (black) and S6 (green). A linear regression was fit to the data to give calculated slopes of 9.9 and 3.6 kcal/mol per amino acid for the tape measure and S6, respectively (correlation coefficients were 0.95 and 0.97, respectively). (B) Assignment of locations for cysteines 408−429. Each cysteine is indicated as residing within or outside the ribosome, according to the results in panel A. The distance of the engineered cysteine from the PTC is listed for each residue. The nascent peptide chain is not drawn to scale.

from this point for the tape measure to emerge from the ribosomal tunnel, a distance of 15−17 Å. For S6, it takes 10−11 residues to traverse the same distance, i.e., ~1.5 Å per amino acid, which describes an α-helix. Thus, it is likely that the S6 segment between residues 418 and 408 is an α-helix.

One possible explanation for this observation is that if the N-terminus of S6 is compact, then it might block the accessibility of the C-terminus to PEG-MAL. Such a scenario would produce an apparent significant right shift of the bottom of the length dependence curve shown in Figure 9A. This is not observed. The C-terminus, whether blocked or unblocked, must be extended according to the data in Figure 9A. Another possible reason for the apparent difference in compactness between the top and bottom of S6 is their different locations in the ribosomal tunnel. To evaluate this possibility, we examined the top and bottom of S6 as separate cassettes placed into the same context in the tape measure and assessed their ability to retract border residue C64. We replaced 11 residues in the tape measure containing C64 with either residues 408−418 or residues 419−429 and compared pegylation of border residue C64 in these two constructs with that of C64 in the unsubstituted tape measure and in Ala10 (Figure 10A). Because 64C is distal to the putative compact region, this strategy has the added benefit of obviating the issue of blocked accessibility of a proximal, more internally located segment. Figure 10B shows that segment 419−429 is more pegylated (less compact) than segment 408−418 ($P = 0.03$, Student's *t* test). Both segments are now located identically near the PTC (only two amino acids away). These results confirm the conclusions drawn from Figure 9 that the two segments of S6 have different extents of compact structure. Segment 408−418 (top of S6) can form a structure that is significantly more compact than the extended, unsubstituted C64 tape measure ($P = 0.002$), and yet less compact than Ala10 ($P = 0.02$). Segment 419−429 (bottom of S6) is significantly less compact than the Ala10 ($P < 0.001$), and yet more compact than the extended C64 tape measure ($P = 0.01$). Thus, compared with the results in Figure 9, these results suggest that the location of the segments in the nascent peptide (and, therefore, the ribosomal tunnel) influences the equilibrium between compact and unfolded states. Moreover, the relative compaction cannot be explained solely by peptide hydrophobicity. Using a relative hydrophobicity scale (Wimley-White, http://blanco.biomol.uci.edu/hydrophobicity_scales.html), we calculated the relative hydrophobicities to be 7.35, −3.38, −0.80, and 5.14 kcal/mol for the 11-residue cassette in the tape measure, the bottom of S6 (residues 419−429), the top of S6 (residues 408−418), and Ala10, respectively. The most hydrophobic segment, the bottom of S6 (residues 419−429), is less compact than Ala10 and the top of S6. Ala10, which is not very hydrophobic, is the most compact. Hydrophobicity does not correlate with the compaction results, suggesting that hydrophobicity alone does not determine compactness, but rather secondary structure does.

DISCUSSION

The transmembrane segments of mature voltage-gated K^+ channels are helical (*1*−*6*). We presume that secondary

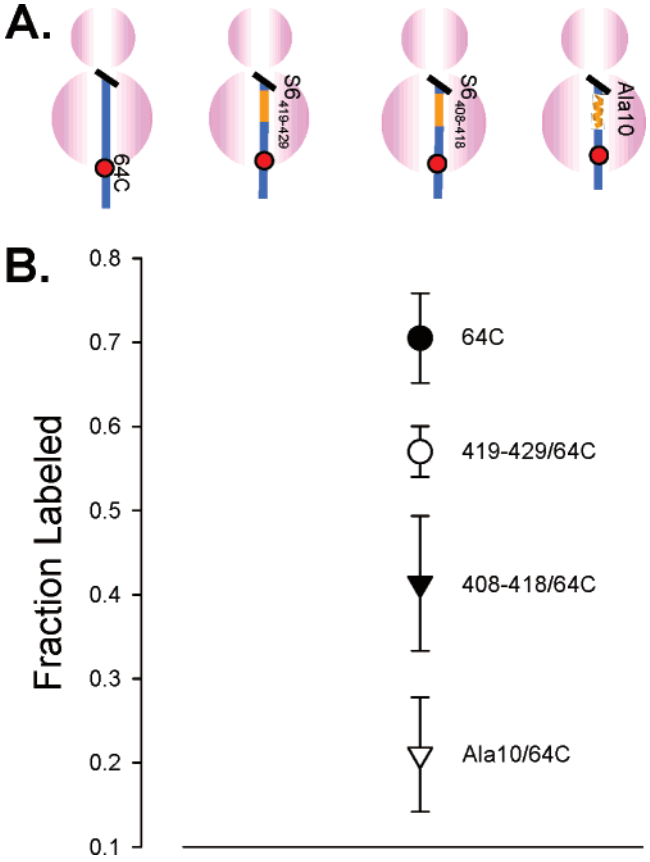

FIGURE 10: Substitution of S6 residues into the tape measure. (A) Cartoons of substituted C64 tape measures. All constructs are the C64 tape measure (described in Figures 3 and 6) in which residues have been replaced with segment 419−429 of S6, segment 408−418 of S6, or 10 consecutive alanines (Ala10). The engineered C64 is colored red; the substituted segments are indicated by the orange bar (S6 segments 408−418 and 419−429) and orange helix (Ala10), and the nascent peptide is colored blue and is not drawn to scale. Note that C64 is shown relatively retracted: 419−429, 408−418 < Ala10, based on the results and implications of Figures 6 and 9A. (B) Fraction of peptide pegylated. Each construct was translated and pegylated as described in the legend of Figure 4. The maximum fractions pegylated are 0.71 ± 0.05 ($n = 4$), 0.57 ± 0.03 ($n = 3$), 0.41 ± 0.08 ($n = 3$), and 0.21 ± 0.07 ($n = 4$) for the unsubstituted C64 tape measure, segment 419−429, segment 408−418, and Ala10, respectively. All values are means ± the standard deviation.

structure is acquired at stages prior to or during insertion of these segments into the ER membrane. The rationale is that Kv channels must correctly assemble into tetramers in the ER to pass quality control and exit (*35*, *36*). This requires correct secondary, tertiary, and quaternary folding. We examined the earliest possible stages for such acquisition, namely, biogenesis of the nascent channel peptide inside the ribosomal exit tunnel. Our first task, however, was to define the functional length of this tunnel and confirm the validity of our experimental approach. We created a molecular tape measure and chose a variant of the cysteine accessibility method (*27*, *28*). We draw three conclusions regarding our experimental approach. First, accessibility measurements faithfully report the compact structure of nascent peptides inside the ribosome. Second, the exit tunnel is an aqueous pore, consistent with previous findings (*17*, *37*). Third, the functional length of the ribosomal tunnel, 99−112 Å (calculated for a range of 3.0−3.4 Å per residue for an all-extended conformation), is similar to, or slightly longer than, the anatomical length of 100 Å (*8*). This agrees with previous results derived from protease protection assays (*38*, *39*).

The first conclusion is based on two findings. First, both rates and the final extent of pegylation are well-behaved monotonic functions of length of the intraribosomal nascent peptide, while those residues that cannot be pegylated can be modified by small maleimides. This shows we are measuring sterically determined accessibility and not reactivity (see also ref *17*). Second, polyalanine replacement of tape measure residues decreases the final extent of labeling of a terminal reporter cysteine. Alanine is the amino acid residue that maximally stabilizes α-helices (*40*); thus, it is likely that the compact structure generated in the polyalanine-substituted construct inside the ribosomal tunnel is an α-helix. Our results are consistent with those obtained for a polyalanine string inserted into a Semliki Forest virus (SFV) capsid protease domain (Cp), which was also concluded to form an α-helix inside the ribosomal tunnel (*16*). We draw the second conclusion, that a high dielectric (i.e., aqueous environment) exists inside the tunnel, because modification by maleimides requires generation of a thiolate ion, which does not occur at low dielectric (*28*). The third conclusion is that the functional length is similar to, or slightly longer than, the anatomical length. The slightly longer distance could reflect accessory proteins normally present at the mouth of the exit tunnel but absent in detergent-derived structures from which the 100 Å length dimension was determined.

In addition to pegylation, we have developed and tested a new probe, CaM-MAL. Its dimensions preclude efficient labeling of residues at a hindered site, e.g., protein−protein interfaces or inside the ribosomal tunnel. The same residue both inside and outside the ribosomal tunnel can be labeled, but at dramatically different rates. CaM-MAL can also be used in accessibility measurements and to identify candidate protein−protein interfaces.

Compaction of nascent peptide inside the ribosome has been implicated previously from five types of assays: protease protection, enzymatic activity of nascent proteins, antibody binding, glycosylation, and fluorescence energy transfer (FRET) (*14*, *15*, *18*, *19*, *38*, *39*, *41*). The limitations of these approaches have been discussed previously (*17*). The cysteine accessibility method presented here exploits the small side chain length of a cysteine and allows changes in chain length to be resolved over a range from ~3 Å to tens of angstroms.

S6 Transmembrane Segment. We have recently shown that helical portions of the cytosolic T1 domain of Kv channels acquire some compact structure inside the tunnel (*17*), but what of transmembrane segments? The S6 accessibility results suggest that some portions of S6 also acquire compact, likely helical, structure inside the ribosomal tunnel.

For residues 408−418, the length-dependent extent of pegylation is significantly right-shifted from that of the tape measure and has a shallower slope. Twice as many amino acids are required for the emergence of accessible cysteines, indicating an α-helix between residues 408 and 418. This slope is not abrupt, but gradual, which is to be expected and has been observed previously for the T1 domain of Kv1.3 (*17*) and for the Cp domain of SFV (*16*). In the case of T1 and the studies herein, the method used was accessibility to PEG-MAL, whereas the method for the Cp domain was autocatalytic cleavage of the folded emergent peptide. In both

cases, heterogeneous secondary structure formation could produce a gradual slope. In addition, the accessibility measurements depend on the depth in the tunnel of the cysteine; i.e., the modification rate depends on the frequency and efficiency of collision between PEG-MAL and cysteine. For a small reagent, such as NEM or PDM, we achieve complete labeling deep within the tunnel. However, competing reactions (e.g., oxidation) will prevail when the pegylation reaction is slow. The probability of modification is $\alpha/(\alpha + \beta)$, where α is the rate of pegylation and β is the rate of competing reactions. Moreover, the calmodulation experiments eliminate the possibility that some of the cysteines reside outside the tunnel and some inside the tunnel. If heterogeneity underlies the gradual slope of length-dependent pegylation, the heterogeneity can occur only inside the tunnel. Nonetheless, the slope and shift of the length dependence of accessibility indicate compaction. For residues 419−447, the length dependence of pegylation is similar to that of the tape measure.

The pegylation results may be further analyzed by assuming that the fraction pegylated reflects a pseudoequilibrium population of accessible versus inaccessible residues. This allows us to calculate a more universally useful quantity, an apparent free energy, with the equation $\Delta G' = -RT \ln[F_{PEG}/(1 - F_{PEG})]$, where F_{PEG} is the fraction of peptide pegylated. From the data in Figure 9A (inset), the free energy is linearly dependent on the length of the chain in the tunnel. The slope ($\Delta\Delta G'$ per amino acid) of 9.9 kcal/mol per amino acid for the tape measure versus a shallower slope of 3.6 kcal/mol per amino acid for S6 indicates the latter is more compact. The $\Delta\Delta G'$ per amino acid can be used to evaluate the relative compactness of a nascent peptide.

Two factors may underlie the different outcomes for the N- and C-terminal regions of S6: helix propensity of the peptide and zones of compaction inherent to the ribosomal tunnel. Helix propensity is sequence specific and determines whether compact structures form in the ribosomal−translocon complex (*14*). Analysis of the S6 sequence using the AGADIR helix propensity algorithm (*32*) indicates that the N-terminal half of S6 has a relatively higher propensity (10-fold) than the C-terminal half of S6. The observed experimental and theoretical differences between the N- and C-terminal halves of S6 are consistent with the presence of a nonhelical stretch, the PVP motif, in the C-terminus of the Kv1 family (*3*, *6*, *30*). Compactness appears to correlate with secondary structure and not with hydrophobicity alone, as the C-terminal half of S6 is more hydrophobic than either the N-terminal half or Ala10 yet the least compact (Figure 10). In addition, consistent with the results in Figures 9 and 10, there may be distinct zones of compaction in the tunnel (also from unpublished data of J. Lu and C. Deutsch).

At least one provocative issue is raised by the S6 results. If a helix, which is ~10 Å in diameter, is formed at the PTC, then how does it pass through constricted regions ≤10 Å in diameter that lie between the PTC and the exit port? One possibility is that the nascent peptide partially unfolds along the way; another is that the ribosome dimensions are dynamic. Precedence for both scenarios exists (*15*, *42*, *43*).

In the presence of membranes, however, a transmembrane segment appears to preserve secondary structure as the nascent peptide progresses through the ribosomal tunnel (*15*). One reason could be the presence of chaperones and critical accessory factors. Another could be the binding of the ribosome to the ER membrane. Each could signal changes in the ribosome interior with consequences for nascent peptide folding. Our experiments with S6 cannot be carried out in the presence of membranes because the translocon prevents access of PEG to the ribosomal tunnel and its exit port. Nor can we obviate this problem by solubilization in nondenaturing detergent (e.g., $C_{12}M$) because the translocon remains intact and attached tightly to the ribosome under such conditions (see Figure 8A,C). Thus, these studies could be carried out only in the absence of membranes. In the presence of membranes, compaction may have different characteristics because of signals from the translocon. Nonetheless, a positive result (i.e., evidence of compaction) is meaningful and suggests that secondary structure can be acquired inside the ribosomal tunnel for a Kv channel transmembrane segment. This conclusion is confirmed by the results shown in Figure 10, in which the two regions of S6, which are helical in the final mature Kv channel, manifest a compact structure when separately expressed in identical locations of the tape measure (i.e., locations in the ribosomal tunnel).

Mechanisms of Helix Induction. What governs compaction and helix formation inside the ribosome? Factors and conditions that promote backbone hydrogen bonding stabilize helix formation. Solvent-exposed hydrogen-bonded helices still interact strongly with water, and nonpolar side chains weaken this interaction (*44*). The latter effect may be a major determinant for helix vis-à-vis β-structure propensities. Given a specific amino acid sequence, why will certain regions inside the ribosomal tunnel promote helix formation while others do not? Several possibilities may be considered. First, the nascent peptide could be transiently exposed to nonpolar patches on the wall of the tunnel in different regions of the ribosomal tunnel (*20*, *45*). In chaperonin models, a cavity with dynamically changing hydrophobicity more efficiently promotes tertiary folding in proteins (*46*, *47*). Could such principles apply to secondary structure formation inside the ribosomal tunnel? A second possibility is that water could be differentially sequestered (e.g., by RNA) inside the tunnel. Another possibility is that secondary and tertiary structure formation may be coupled (*48*). Secondary structures are weak, but can be stabilized by tertiary interactions made with the rest of the protein in the transition state [a "tertiary contact-assisted" mechanism (*49*)]. Although tertiary folding of large nascent domains inside the tunnel is precluded by the size of the tunnel (*16*, *17*, *41*), ribosomal proteins could provide tertiary contact assistance along the length of the tunnel. Nascent peptide−ribosomal protein interactions exist (*15*, *50*) (A. Kosolapov and C. Deutsch, unpublished data) and might contribute to specific zones of induction and stabilization of helices. Such a hypothesis could account for the apparent nonuniform compaction of the S6 segment along the tunnel.

Another consideration that bears on the mechanism of compaction is confinement of a polypeptide to a restricted compartment. This reduces the conformational entropy of the folding reaction, shifting the equilibrium from an unfolded state to a folded state, and has been proposed to promote protein folding in the GroEL−GroES complex (*51*−*54*). In the case of the ribosomal tunnel, the protein and the confining cage are of comparable size, which would be

predicted to have a large entropic effect (*54*). We speculate that the small diameter of the ribosomal tunnel entropically drives compaction and does so differentially along the tunnel. A recent theoretical calculation of polymer folding in a noncontained system suggests helix formation is entropically driven (*55*).

The length of a hydrophobic stretch of nascent peptide has also been postulated to be a determinant of helix formation of transmembrane segments (*15*). Specifically, more than 10 residues are required for compaction. However, Ala10, which is neither very hydrophobic (*56*) nor long, confers a compact structure on the Ala10 peptide. It is possible that the strong helix propensity of Ala10 versus a weaker propensity for the transmembrane segment used by Woolhead et al. (*15*) overrides Woolhead et al.'s injunction against short, hydrophobic stretches. However, segment 408−418 in S6 is 11 amino acids in length, with a helix propensity weaker than that of Ala10, yet it contributes a compact structure to the nascent peptide. Most natural transmembrane segments have helices with lower helix propensities than Ala10 but enough length, e.g., ∼20 amino acids, to span the bilayer. Some combination of hydrophobicity and length may contribute to compaction within the ribosomal tunnel.

Structure acquisition is a coordinated process. When it goes awry, it can lead to protein misfolding, the basis of many disease-producing channelopathies. Our studies begin to shed light on some of the early steps of channel biogenesis, and thus bear on the etiology of these pathological conditions.

ACKNOWLEDGMENT

We thank Y. Goldmann for giving us the P66C calmodulin clone and S. W. Englander, L. Mayne, J. Lear, and R. Horn for helpful discussions and insights. We thank R. Horn, A. Kosolapov, S. W. Englander, and J. Lear for critical reading of the manuscript.

REFERENCES

1. Monks, S. A., Needleman, D. J., and Miller, C. (1999) Helical structure and packing orientation of the S2 segment in the Shaker K^+ channel, *J. Gen. Physiol. 113*, 415−423.
2. Hong, K. H., and Miller, C. (2000) The lipid−protein interface of a Shaker K^+ channel, *J. Gen. Physiol. 115*, 51−58.
3. Hackos, D. H., Chang, T. H., and Swartz, K. J. (2002) Scanning the intracellular S6 activation gate in the shaker K^+ channel, *J. Gen. Physiol. 119*, 521−532.
4. Li-Smerin, Y., Hackos, D. H., and Swartz, K. J. (2000) A localized interaction surface for voltage-sensing domains on the pore domain of a K^+ channel, *Neuron 25*, 411−423.
5. Li-Smerin, Y., Hackos, D. H., and Swartz, K. J. (2000) α-Helical structural elements within the voltage-sensing domains of a K^+ channel, *J. Gen. Physiol. 115*, 33−50.
6. Jiang, Y., Lee, A., Chen, J., Ruta, V., Cadene, M., Chait, B. T., and MacKinnon, R. (2003) X-ray structure of a voltage-dependent K^+ channel, *Nature 423*, 33−41.
7. Ban, N., Nissen, P., Hansen, J., Moore, P. B., and Steitz, T. A. (2000) The complete atomic structure of the large ribosomal subunit at 2.4 Å resolution, *Science 289*, 905−920.
8. Nissen, P., Hansen, J., Ban, N., Moore, P. B., and Steitz, T. A. (2000) The structural basis of ribosome activity in peptide bond synthesis, *Science 289*, 920−930.
9. Menetret, J. F., Neuhof, A., Morgan, D. G., Plath, K., Radermacher, M., Rapoport, T. A., and Akey, C. W. (2000) The structure of ribosome-channel complexes engaged in protein translocation, *Mol. Cell 6*, 1219−1232.
10. Beckmann, R., Spahn, C. M., Eswar, N., Helmers, J., Penczek, P. A., Sali, A., Frank, J., and Blobel, G. (2001) Architecture of the protein-conducting channel associated with the translating 80S ribosome, *Cell 107*, 361−372.
11. Creighton, T. E. (1993) in *Proteins*, pp 171−199, W. H. Freeman and Company, New York.
12. Eaton, W. A., Munoz, V., Hagen, S. J., Jas, G. S., Lapidus, L. J., Henry, E. R., and Hofrichter, J. (2000) Fast kinetics and mechanisms in protein folding, *Annu. Rev. Biophys. Biomol. Struct. 29*, 327−359.
13. Fedorov, A. N., and Baldwin, T. O. (1998) Protein folding and assembly in a cell-free expression system, *Methods Enzymol. 290*, 1−17.
14. Mingarro, I., Nilsson, I., Whitley, P., and von Heijne, G. (2000) Different conformations of nascent polypeptides during translocation across the ER membrane, *BMC Cell Biol. 1*, 3.
15. Woolhead, C. A., McCormick, P. J., and Johnson, A. E. (2004) Nascent membrane and secretory proteins differ in FRET-detected folding far inside the ribosome and in their exposure to ribosomal proteins, *Cell 116*, 725−736.
16. Kowarik, M., Kung, S., Martoglio, B., and Helenius, A. (2002) Protein folding during cotranslational translocation in the endoplasmic reticulum, *Mol. Cell 10*, 769−778.
17. Kosolapov, A., Tu, L., Wang, J., and Deutsch, C. (2004) Structure Acquisition of the T1 Domain of Kv1.3 During Biogenesis, *Neuron 44*, 295−307.
18. Hardesty, B., and Kramer, G. (2001) Folding of a nascent peptide on the ribosome, *Prog. Nucleic Acid Res. Mol. Biol. 66*, 41−66.
19. Matlack, K. E., and Walter, P. (1995) The 70 carboxyl-terminal amino acids of nascent secretory proteins are protected from proteolysis by the ribosome and the protein translocation apparatus of the endoplasmic reticulum membrane, *J. Biol. Chem. 270*, 6170−6180.
20. Liao, S., Lin, J., Do, H., and Johnson, A. E. (1997) Both lumenal and cytosolic gating of the aqueous ER translocon pore are regulated from inside the ribosome during membrane protein integration, *Cell 90*, 31−41.
21. Fersht, A. R. (1997) Nucleation mechanisms in protein folding, *Curr. Opin. Struct. Biol. 7*, 3−9.
22. Shakhnovich, E. I. (1997) Theoretical studies of protein-folding thermodynamics and kinetics, *Curr. Opin. Struct. Biol. 7*, 29−40.
23. Fedorov, A. N., and Baldwin, T. O. (1995) Contribution of cotranslational folding to the rate of formation of native protein structure, *Proc. Natl. Acad. Sci. U.S.A. 92*, 1227−1231.
24. Kosolapov, A., and Deutsch, C. (2003) Folding of the voltage-gated K^+ channel T1 recognition domain, *J. Biol. Chem. 278*, 4305−4313.
25. Fedorov, A. N., and Baldwin, T. O. (1997) Cotranslational protein folding, *J. Biol. Chem. 272*, 32715−32718.
26. Lu, J., Robinson, J. M., Edwards, D., and Deutsch, C. (2001) T1-T1 interactions occur in ER membranes while nascent Kv peptides are still attached to ribosomes, *Biochemistry 40*, 10934−10946.
27. Lu, J., and Deutsch, C. (2001) Pegylation: A method for assessing topological accessibilities in Kv1.3, *Biochemistry 40*, 13288−13301.
28. Karlin, A., and Akabas, M. H. (1998) Substituted-cysteine accessibility method, *Methods Enzymol. 293*, 123−145.
29. Yellen, G. (2002) The voltage-gated potassium channels and their relatives, *Nature 419*, 35−42.
30. del Camino, D., Holmgren, M., Liu, Y., and Yellen, G. (2000) Blocker protection in the pore of a voltage-gated K^+ channel and its structural implications, *Nature 403*, 321−325.
31. Kreusch, A., Pfaffinger, P. J., Stevens, C. F., and Choe, S. (1998) Crystal structure of the tetramerization domain of the *Shaker* potassium channel, *Nature 392*, 945−948.
32. Munoz, V., and Serrano, L. (1997) Development of the multiple sequence approximation within the AGADIR model of α-helix formation: Comparison with Zimm-Bragg and Lifson-Roig formalisms, *Biopolymers 41*, 495−509.
33. Picking, W. D., Picking, W. L., Odom, O. W., and Hardesty, B. (1992) Fluorescence characterization of the environment encountered by nascent polyalanine and polyserine as they exit *Escherichia coli* ribosomes during translation, *Biochemistry 31*, 2368−2375.
34. Bernabeu, C., and Lake, J. A. (1982) Nascent polypeptide chains emerge from the exit domain of the large ribosomal subunit: Immune mapping of the nascent chain, *Proc. Natl. Acad. Sci. U.S.A. 79*, 3111−3115.
35. Deutsch, C. (2003) The birth of a channel, *Neuron 40*, 265−276.

36. Deutsch, C. (2002) Potassium channel ontogeny, *Annu. Rev. Physiol. 64*, 19−46.
37. Hamman, B. D., Chen, J. C., Johnson, E. E., and Johnson, A. E. (1997) The aqueous pore through the translocon has a diameter of 40−60 Å during cotranslational protein translocation at the ER membrane, *Cell 89*, 535−544.
38. Malkin, L. I., and Rich, A. (1967) Partial resistance of nascent polypeptide chains to proteolytic digestion due to ribosomal shielding, *J. Mol. Biol. 26*, 329−346.
39. Blobel, G., and Sabatini, D. D. (1970) Controlled proteolysis of nascent polypeptides in rat liver cell fractions. I. Location of the polypeptides within ribosomes, *J. Cell Biol. 45*, 130−145.
40. O'Neil, K. T., and DeGrado, W. F. (1990) A thermodynamic scale for the helix-forming tendencies of the commonly occurring amino acids, *Science 250*, 646−651.
41. Kramer, G., Ramachandiran, V., and Hardesty, B. (2001) Cotranslational folding: Omnia mea mecum porto? *Int. J. Biochem. Cell Biol. 33*, 541−553.
42. Berisio, R., Schluenzen, F., Harms, J., Bashan, A., Auerbach, T., Baram, D., and Yonath, A. (2003) Structural insight into the role of the ribosomal tunnel in cellular regulation, *Nat. Struct. Biol. 10*, 366−370.
43. Gilbert, R. J., Fucini, P., Connell, S., Fuller, S. D., Nierhaus, K. H., Robinson, C. V., Dobson, C. M., and Stuart, D. I. (2004) Three-dimensional structures of translating ribosomes by Cryo-EM, *Mol. Cell 14*, 57−66.
44. Baldwin, R. L. (2002) Relation between peptide backbone solvation and the energetics of peptide hydrogen bonds, *Biophys. Chem. 101−102*, 203−210.
45. DeGrado, W. F., and Lear, J. D. (1985) Induction of Peptide Conformation at Apolar/Water Interfaces. 1. A study with model peptides of defined hydrophobic periodicity, *J. Am. Chem. Soc. 107*, 7684−7689.
46. Chan, H. S., and Dill, K. A. (1996) A simple model of chaperonin-mediated protein folding, *Proteins 24*, 345−351.
47. Betancourt, M. R., and Thirumalai, D. (1999) Exploring the kinetic requirements for enhancement of protein folding rates in the GroEL cavity, *J. Mol. Biol. 287*, 627−644.
48. Uversky, V. N., and Fink, A. L. (2002) The chicken-egg scenario of protein folding revisited, *FEBS Lett. 515*, 79−83.
49. Daggett, V., and Fersht, A. R. (2003) Is there a unifying mechanism for protein folding? *Trends Biochem. Sci. 28*, 18−25.
50. Nakatogawa, H., and Ito, K. (2002) The ribosomal exit tunnel functions as a discriminating gate, *Cell 108*, 629−636.
51. Minton, A. P. (1992) Confinement as a determinant of macromolecular structure and reactivity, *Biophys. J. 63*, 1090−1100.
52. Zhou, H. X., and Dill, K. A. (2001) Stabilization of proteins in confined spaces, *Biochemistry 40*, 11289−11293.
53. Klimov, D. K., Newfield, D., and Thirumalai, D. (2002) Simulations of β-hairpin folding confined to spherical pores using distributed computing, *Proc. Natl. Acad. Sci. U.S.A. 99*, 8019−8024.
54. Takagi, F., Koga, N., and Takada, S. (2003) How protein thermodynamics and folding mechanisms are altered by the chaperonin cage: Molecular simulations, *Proc. Natl. Acad. Sci. U.S.A. 100*, 11367−11372.
55. Snir, Y., and Kamien, R. D. (2005) Entropically driven helix formation, *Science 307*, 1067.
56. Nilsson, I., Johnson, A. E., and von Heijne, G. (2003) How hydrophobic is alanine? *J. Biol. Chem. 278*, 29389−29393.

BI050372Q